



Performance of the Muon Identification at LHCb

The LHCb MuonID group [†]

Abstract

The performance of the muon identification in LHCb is extracted from data using muons and hadrons produced in $J/\psi \rightarrow \mu^+\mu^-$, $\Lambda^0 \rightarrow p\pi^-$ and $D^{*+} \rightarrow \pi^+D^0(K^-\pi^+)$ decays. The muon identification procedure is based on the pattern of hits in the muon chambers. A momentum dependent binary requirement is used to reduce the probability of hadrons to be misidentified as muons to the level of 1%, keeping the muon efficiency in the range of 95-98%. As further refinement, a likelihood is built for the muon and non-muon hypotheses. Adding a requirement on this likelihood that provides a total muon efficiency at the level of 93%, the hadron misidentification probabilities are below 0.6%.

(To be submitted to JINST)

[†]Authors are listed on the following pages.

The LHCb MuonID Group

F. Archilli¹, W. Baldini², G. Bencivenni¹, N. Bondar³, W. Bonivento⁴, S. Cadeddu⁴, P. Campana¹, A. Cardini⁴, M. Carletti¹, P. Ciambrone¹, X. Cid Vidal⁵, C. Deplano⁴, P. De Simone¹, M. Frosini⁶, S. Furcas^{1,a}, E. Furfaro⁷, M. Gandelman⁸, J.A. Hernando Morata⁹, G. Graziani⁶, A. Lai⁴, G. Lanfranchi¹, J.H. Lopes⁸, O. Maev³, G. Manca⁴, G. Martellotti⁷, A. Massafferri¹⁰, D. Milanese¹¹, R. Oldeman^{4,13}, M. Palutan¹, G. Passaleva⁶, D. Pinci⁷, E. Polycarpo⁸, R. Santacesaria⁷, E. Santovetti^{12,14}, A. Sarti^{1,16}, A. Satta¹², B. Schmidt⁵, B. Sciascia¹, F. Soomro¹, A. Sciubba^{7,16}, S. Vecchi².

¹*INFN - Laboratori Nazionali di Frascati, Italy*

²*Sezione INFN di Ferrara, Ferrara, Italy*

³*Petersburg Nuclear Physics Institute, Gatchina, St-Petersburg, Russia*

⁴*Sezione INFN di Cagliari, Cagliari, Italy*

⁵*European Organisation for Nuclear Research (CERN), Geneva, Switzerland*

⁶*Sezione INFN di Firenze, Firenze, Italy*

⁷*Sezione INFN di Roma, Roma, Italy* ⁸*Instituto de Física, Universidade Federal do Rio de Janeiro (UFRJ), Brasil*

⁹*Universidade de Santiago de Compostela, Santiago de Compostela, Spain*

¹⁰*Centro Brasileiro de Pesquisas Físicas (CBPF), Rio de Janeiro, Brasil*

¹¹*Sezione INFN di Bari, Bari, Italy*

¹²*Sezione INFN di Roma Tor Vergata, Roma, Italy*

¹³*Università di Cagliari, Cagliari, Italy*

¹⁴*Università di Firenze, Firenze, Italy*

¹⁵*Università di Roma Tor Vergata, Roma, Italy*

¹⁶*Sapienza, Università di Roma, Roma, Italy*

^a*Now at Sezione INFN di Milano, Milano, Italy*

Contents

| | | |
|----------|---|-----------|
| 1 | Introduction | 1 |
| 2 | The LHCb experiment and the muon system | 1 |
| 3 | The muon identification procedure | 3 |
| 3.1 | IsMuon binary selection | 3 |
| 3.2 | Muon and non-muon likelihoods | 4 |
| 3.3 | Combined likelihoods | 5 |
| 3.4 | Discriminating variable based on hits sharing | 6 |
| 4 | Method for the extraction of efficiencies | 7 |
| 4.1 | Selection of control samples | 7 |
| 4.2 | Efficiency evaluation | 8 |
| 5 | Results | 8 |
| 5.1 | IsMuon performance | 8 |
| 5.2 | Muon likelihoods | 12 |
| 5.3 | Combined likelihoods | 12 |
| 5.4 | Performance of selections based on hits sharing | 13 |
| 5.5 | Systematic checks | 14 |
| 6 | Conclusions | 16 |

1 Introduction

LHCb [1] is a dedicated heavy flavour experiment, designed to exploit the high $pp \rightarrow c\bar{c}$ and $pp \rightarrow b\bar{b}$ cross-sections at the LHC in order to perform precision measurements of CP violation and rare decays. Muons are present in the final state of many of the key decays, sensitive to new physics, as shown, for example, in [2, 3, 4, 5, 6, 7], among others. Moreover, they play a crucial role in the determination of the flavor tagging of the neutral B mesons and are also present in the signatures of interesting electroweak and strong processes. The muon identification procedure must provide high muon efficiency while keeping the incorrect identification probability of hadrons as muons (misidentification probabilities) at the lowest possible level. The pion misidentification is one of the major sources of combinatoric background for decays with muons in the final state. It is also important to keep the other hadron misidentification probabilities at low levels so that rare decays can be separated from more abundant hadronic decays with similar or identical topology.

This paper presents the performance of the muon identification in LHCb, obtained from the data recorded in 2011, corresponding to approximately 1 fb^{-1} . In Section 2, a brief description of the LHCb spectrometer and the muon detection system is given. The muon identification algorithm is discussed in Section 3. The method used to extract the muon efficiency and the misidentification probability from data is explained in Section 4. Finally, the performance results are presented in Section 5, followed by the conclusions in Section 6.

2 The LHCb experiment and the muon system

The LHCb detector [1] is a single-arm forward spectrometer. A vertex locator (VELO) determines with high precision the positions of the vertices of pp collisions (PVs) and the decay vertices of long-lived particles. The tracking system includes a silicon strip detector located in front of a dipole magnet with an integrated field of about 4 Tm, and a combination of silicon strip detectors and straw drift chambers placed behind the magnet. The momentum of charged particles is determined with a resolution of $\sigma_p/p \sim 0.4(0.6)\%$ at a momentum scale of 3(100) GeV/ c . Charged hadron identification is achieved with two ring-imaging Cherenkov (RICH) detectors. The calorimeter system consists of a scintillator pad detector, a preshower, an electromagnetic calorimeter and a hadronic calorimeter. It identifies high transverse energy hadron, electron and photon candidates and provides information for the trigger.

The muon system [8] is composed of five stations (M1-M5) of rectangular shape, placed along the beam axis, as shown in Fig. 1. Station M1 is located in front of the calorimeters and is used to improve the transverse momentum measurement in the first level hardware trigger. Stations M2 to M5 are placed downstream the calorimeters and are interleaved with iron absorbers 80 cm thick to select penetrating muons. The total absorber thickness in front of station M2, including the calorimeters, is approximately 6.6 interaction lengths. More than 99% of the total area of the system is equipped with

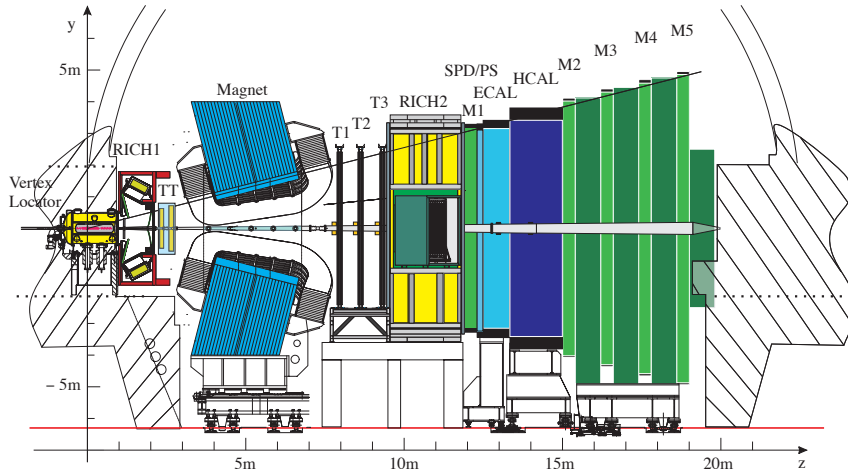


Figure 1: Schematic view of the LHCb experiment. The muon stations are seen as the five green vertical bars, the second one placed just after the calorimeters, shown as the blue rectangles.

41 multi-wire proportional chambers (MWPC) with Ar/CO₂/CF₄(40:55:5) as gas mixture.
 42 Only the inner part of the first station is instrumented with triple-GEM detectors filled
 43 with Ar/CO₂/CF₄(45:15:40).

44 The chambers are positioned to provide with their sensitive area a hermetic geometric
 45 acceptance to high momentum particles coming from the interaction point. In addition,
 46 the chambers of different stations form projective towers pointing to the interaction
 47 point. The detectors provide digital space point measurements of the particle trajectories,
 48 supplying information to the trigger processor and to the data acquisition (DAQ). The
 49 information is obtained by partitioning the detector into rectangular logical pads whose
 50 dimensions define the x, y resolution in the plane perpendicular to the beam axis. Each
 51 station is divided into four regions, R1 to R4 with increasing distance from the beam
 52 axis, as shown in Fig. 2. The linear dimensions of the regions R1, R2, R3, R4, and their
 53 segmentation scale in the ratio 1:2:4:8. Each muon station is designed to perform with an
 54 efficiency above 99% in a 20 ns time window with a noise rate below 1 kHz per physical
 55 channel, which was achieved during operation, as described in [8].

56 The muon system provides information for the selection of high transverse momentum
 57 muons at the trigger level and for the offline muon identification. This document refers
 58 to the latter procedure, which uses only the information from the 4 stations located after
 59 the calorimeters. The muon identification in the trigger system is described in [9].

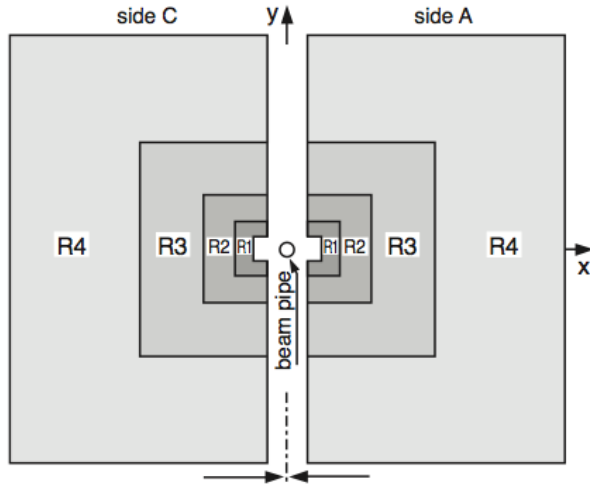


Figure 2: Schematic view of one muon system station (reproduced from [8]).

3 The muon identification procedure

The muon identification strategy can be divided in three steps:

- A loose binary selection of muon candidates based on the penetration of the muons through the calorimeters and iron filters, which provides high efficiency while reducing the misidentification probability of hadrons to the percent level (called IsMuon);
- Computation of a likelihood for the muon and non-muon hypotheses, based on the pattern of hits around the extrapolation to the different muon stations of the charged particles trajectories reconstructed with high precision in the tracking system. The logarithm of the ratio between the muon and non-muon hypotheses is used as discriminating variable and called muDLL.
- Computation of a combined likelihood for the different particle hypotheses, including information from the calorimeter and RICH systems. The logarithm of the ratio between the muon and pion hypotheses is used as discriminating variable and called DLL.

Additionally the number of tracks identified as muons that share a hit with a given muon candidate (called NShared) can be used to further reject false candidates.

3.1 IsMuon binary selection

The binary selection is defined according to the number of stations where a hit is found within a field of interest (FOI) defined around the track extrapolation. The number of stations required to have a muon signal is a function of track momentum (p), as shown in Table 1. The sizes of the fields of interest also depend on the particle momentum

and are defined according to the expected multiple scattering suffered by a muon when traversing the material. The FOI are parameterized separately for the 4 regions of the 4 different stations downstream the calorimeter in both x and y directions according to:

$$\text{FOI} = a + b \times \exp(-c \times p). \quad (1)$$

77 The parameters a , b and c have been determined using muons from a full detector Monte
78 Carlo simulation [10].

| Momentum range | Muon stations |
|--|--------------------------|
| $3 \text{ GeV}/c < p < 6 \text{ GeV}/c$ | M2 and M3 |
| $6 \text{ GeV}/c < p < 10 \text{ GeV}/c$ | M2 and M3 and (M4 or M5) |
| $p > 10 \text{ GeV}/c$ | M2 and M3 and M4 and M5 |

Table 1: Muon stations required to trigger the IsMuon decision as a function of momentum range.

79 For tracks passing the IsMuon requirement, the muon identification can be further
80 improved by a selection based on the logarithm of the ratio between the likelihoods for
81 the muon and non-muon hypotheses (muDLL).

82 3.2 Muon and non-muon likelihoods

83 The likelihoods are computed as the cumulative probability distributions of the average
84 squared distance significance D^2 of the hits in the muon chambers with respect to the
85 linear extrapolation of the tracks from the tracking system. True muons tend to have a
86 much narrower D^2 distribution, close to zero, than the other particles that are incorrectly
87 selected by the IsMuon requirement.

88 The average squared distance significance is defined as:

$$D^2 = \frac{1}{N} \sum_i \left\{ \left(\frac{x_{closest}^i - x_{track}^i}{pad_x^i} \right)^2 + \left(\frac{y_{closest}^i - y_{track}^i}{pad_y^i} \right)^2 \right\} \quad (2)$$

89 where the index i runs over the stations containing hits within the FOI, $(x_{closest}^i, y_{closest}^i)$
90 are the coordinates of the closest hit to the track extrapolation point for each station
91 $(x_{track}^i, y_{track}^i)$ and $pad_{x,y}^i$ correspond to one half of the pad sizes in the x,y directions.
92 The total number of stations containing hits within their FOI is denoted by N .

93 The D^2 distribution for muons depends on the multiple scattering and, therefore, on
94 the momentum (p) and polar angle (θ) distributions of the analyzed sample. In order to
95 avoid a dependence of the muon likelihood on the calibration sample (with particular p
96 and θ), the tuning of the muon likelihood is performed separately in momentum bins and
97 muon detector regions (which correspond to 4 intervals in θ).

98 The likelihood for the non-muon hypothesis is calibrated with the D^2 distribution for
 99 protons, since the other charged hadrons (pions or kaons) selected by IsMuon will present
 100 a D^2 distribution with a component identical to the protons and a component very similar
 101 to the true muons, due to decays in flight before the calorimeter. For protons, the hits
 102 in the muon system found around the track extrapolation are essentially due to three
 103 sources: hits from punch-through [11] protons, hits from true muons pointing to the same
 104 direction of the proton or random hits. The last two are at first order uncorrelated to
 105 the proton momentum while the first one can present some momentum dependence, less
 106 important however than the dependence expected for muons. Hence, the tuning of the
 107 non-muon likelihood is merely performed separately for the 4 muon system regions, due
 108 to their different granularity.

109 The likelihood for the muon (or non-muon) hypothesis is then defined, for each candi-
 110 date, as the integral of the calibrated muon (or proton) D^2 probability density function
 111 from 0 to the measured value, D_0^2 .

112 The results presented in this document are obtained with a muon likelihood calibrated
 113 with muons from $J/\psi \rightarrow \mu^+\mu^-$ decays selected from the data taken in 2010, as described
 114 in Section 4. The non-muon likelihood has been calibrated with a simulated sample of
 115 decays $\Lambda^0 \rightarrow p\pi^-$.

116 The D^2 distributions for muons, protons, pions and kaons obtained from data are
 117 shown in Fig. 3(a). The distributions of the logarithm of the ratio between the muon
 118 and non-muon hypotheses (muDLL) are shown in Fig. 3(b). More details about the
 119 selection of the particles used to make these plots and to extract the performance are
 120 given in Section 4.

121 3.3 Combined likelihoods

122 The muon and non-muon likelihoods presented in Section 3.2 can be combined with the
 123 likelihoods provided by the RICH systems and the calorimeters to improve the muon
 124 identification performance.

125 The Cherenkov angles measured in the two RICH detectors are combined with the
 126 track momentum using an overall event log-likelihood algorithm. For each track in the
 127 event, a likelihood is assigned to each of the different mass hypotheses (electron, muon,
 128 pion, kaon and proton). The RICH likelihood can differentiate between muon and other
 129 particles in particular at low momentum, below 5 GeV/c [12].

130 The energy deposition in the calorimeters also allows the evaluation of likelihoods for
 131 the muon (minimum ionizing particle), electron and hadron hypotheses.

132 A combined log-likelihood is then obtained for each track and for each of the different
 133 mass hypotheses by summing the logarithms of the likelihoods obtained using the muon
 134 system, the RICH and the calorimeters. In this computation, the non-muon likelihood
 135 obtained in the muon system is assigned to the electron, pion, kaon and proton hypotheses.
 136 The difference of the combined log-likelihoods for the muon and pion hypotheses (DLL)
 137 is then used to identify the muons.

138 **3.4 Discriminating variable based on hits sharing**

139 Different tracks can be associated to the same muon hits when the matching of tracks
 140 to muon chamber hits is performed. Reducing the number of tracks that share hits can
 141 help to improve the misidentification probability. To use this information, a discriminant
 142 variable named NShared is built for tracks satisfying the IsMuon criteria and a score of 1
 143 is added to a given track if it shares any hits with another one. The score is given to the
 144 track to which the hit is more distant. Selecting muons with NShared=0 is the usual way
 145 to reduce the probability of incorrectly identifying hadrons as muons due to nearby true
 146 muons in high multiplicity events, but looser requirements can also be applied as shown
 147 in Fig. 4.

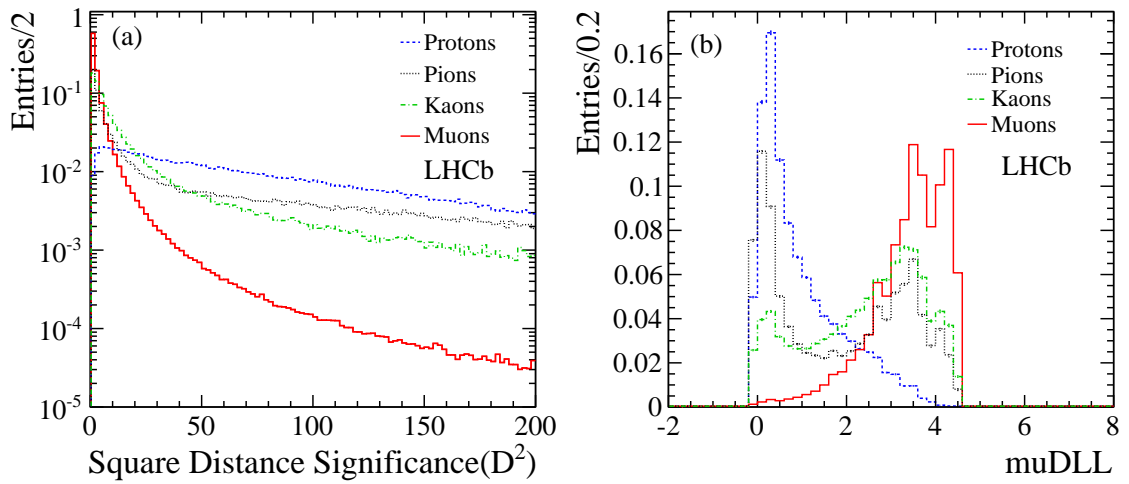


Figure 3: Average square distance significance distributions for muons, protons, pions and kaons (a) and the corresponding muDLL distributions (b).

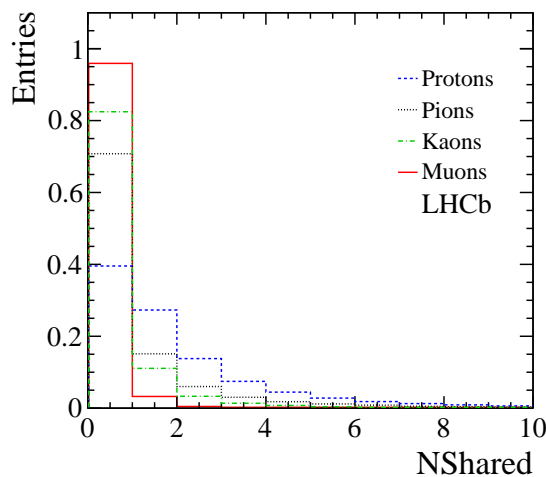


Figure 4: Normalized NShared distributions for muons, protons, kaons and pions.

4 Method for the extraction of efficiencies

In order to extract the performance of the muon identification from data, muon, proton, pion, and kaon candidates are selected with high purity from two body decays using kinematical requirements only. When necessary, the purity is improved by using a *tag and probe technique* where particle identification requirements are applied to one of the tracks (tag) while the other (probe) is used for the computation of the muon efficiency or of the hadron misidentification probability.

4.1 Selection of control samples

An abundant source of muons is provided in the experiment by the $J/\psi \rightarrow \mu^+\mu^-$ decay. By requiring the muons to have a high impact parameter with respect to the primary vertex and the reconstructed J/ψ to have a large flight distance significance and good decay vertex quality, most of the combinatorial background originating from the tracks coming from the primary vertex is removed and the sample gets enriched by $B \rightarrow J/\psi X$ candidates. In order to reduce further the combinatorial background, one of the muons is required to be identified as a muon. This is defined as the *tag* muon, while the one being probed is only required to have $p_T > 0.8 \text{ GeV}/c$.

Protons are selected from the $\Lambda^0 \rightarrow p\pi^-$ decays reconstructed using decay vertex quality criteria and detachment of the decay vertex from the primary one. Besides, the invariant mass obtained by assigning the π mass to the two daughters is required to be out of a window of $20 \text{ MeV}/c^2$ around the nominal K_s^0 mass.

The $D^{*+} \rightarrow \pi^+ D^0$ ($\rightarrow K^- \pi^+$) decays are the source of pions and kaons. Once again relatively high impact parameter is required for the daughters while the D^0 flight direction is required to point to the primary vertex. To evaluate the pion misidentification probability, the tag kaon is selected using a suitable cut on the π - K log-likelihoods difference, based on the RICH information. To evaluate the kaon misidentification probability, the RICH particle identification is used to identify the pion. Quality criteria are used for the D^{*+} and D^0 decay vertices. A window of $25 \text{ MeV}/c^2$ around the nominal D^0 mass is used to exclude the doubly Cabibbo suppressed mode and the K^+K^- and $\pi^+\pi^-$ decay channels.

To avoid potential biases from the trigger requirements, in the J/ψ and Λ^0 samples only events triggered independently on the probe track are used; this condition has to be satisfied at both hardware and software level, as explained in [13]. For the $D^0 \rightarrow K^- \pi^+$ sample, a substantial fraction of the events would be lost by such requirement. Therefore the hardware trigger is required to be activated independently on the probe track (kaon or pion) and the software trigger decision is based on impact parameter and detachment from the primary vertex only, with no particle identification requirement.

After the background subtraction of selected two-body decays, the number of muon, proton, pion and kaon candidates in the 2011 data samples are 2.4, 16.1, 11.7 and 12.3 millions, respectively.

187 4.2 Efficiency evaluation

As a baseline method to evaluate the efficiency ϵ_{muonID} of a generic muon identification requirement denoted in this section by $muonID$ (e.g. IsMuon true or DLL greater than a given cut), is used :

$$\epsilon_{muonID} = \frac{S_{true}}{S_{true} + S_{false}}, \quad (3)$$

where S_{true} and S_{false} are the numbers of signal events satisfying and not satisfying $muonID$, extracted from data using

$$S_{true,false} = N_{true,false} - B_{true,false}. \quad (4)$$

188 $N_{true,false}$ are obtained by counting the number of J/ψ candidates with invariant mass
189 lying within a signal mass window around the J/ψ mass; the number of background
190 events within the same mass window, $B_{true,false}$, is computed by extrapolating to the
191 signal window the mass fit done in the J/ψ sidebands.

192 For the proton misidentification probability, the same method is used. The kaon
193 and pion misidentification probabilities are also obtained with Eq. 3, but $S_{true,false}$ and
194 $B_{true,false}$ are extracted directly from a full fit of the signal and background shapes to the
195 invariant mass distribution of the D^0 candidates.

196 5 Results

197 The muon identification performance is presented in terms of the muon efficiency and
198 hadron misidentification probabilities for the different requirements. In all cases, the
199 performance is evaluated for tracks extrapolated within the geometrical acceptance of the
200 muon detector.

201 5.1 IsMuon performance

202 The efficiency of the IsMuon requirement, ϵ_{IM} , is the efficiency of finding hits within
203 the fields of interest in the muon chambers for tracks extrapolated to the muon system.
204 In Fig. 5, ϵ_{IM} is shown as a function of the muon momentum, for different transverse
205 momentum ranges. A weak dependency with transverse momentum is observed and in
206 particular a drop of $\sim 2\%$ is measured for the lowest p_T interval. This efficiency drop is
207 essentially due to tracks close to the inner edges of region R1 which in principle have their
208 extrapolation points within M1 and M5 acceptance, but are in fact scattered outside the
209 detector. For particles with p_T above 1.7 GeV/c, the efficiency is above 97% in the whole
210 momentum range, from 3 GeV/c to 100 GeV/c. The average efficiency obtained for the
211 μ_{probe} in the J/ψ calibration sample is $\epsilon_{IM} = (98.13 \pm 0.04)\%$, for particles with $p > 3$ GeV
212 and $p_T > 0.8$ GeV/c.

213 The misidentification probabilities $\wp_{IM}(p \rightarrow \mu)$, $\wp_{IM}(\pi \rightarrow \mu)$ and $\wp_{IM}(K \rightarrow \mu)$ are
214 also shown in Fig. 5. The observed decrease of \wp_{IM} with increasing transverse momentum

215 is expected, since tracks with higher transverse momentum traverse the detector at higher
 216 polar angles, in the lower occupancy regions. The proton misidentification probability is
 217 smaller than 0.5% for all p_T ranges and momentum above 30 GeV/c. It drops quickly with
 218 momentum for the lowest p_T ranges, reaching a plateau at about 30-40 GeV/c. The pion
 219 and kaon misidentification probabilities have a similar behavior, increasing with decreasing
 220 p_T . Above 40 GeV/c, the pion misidentification probability is almost at the level of the
 221 proton misidentification probability. At low momentum, decays in flight are the dominant
 222 source of incorrect identification, as can be seen from the difference between the pion/kaon
 223 and proton curves. While the proton misidentification probability, within the p_T intervals
 224 chosen, lies within 0.1-1.3%, the pion and kaon misidentification probabilities are within

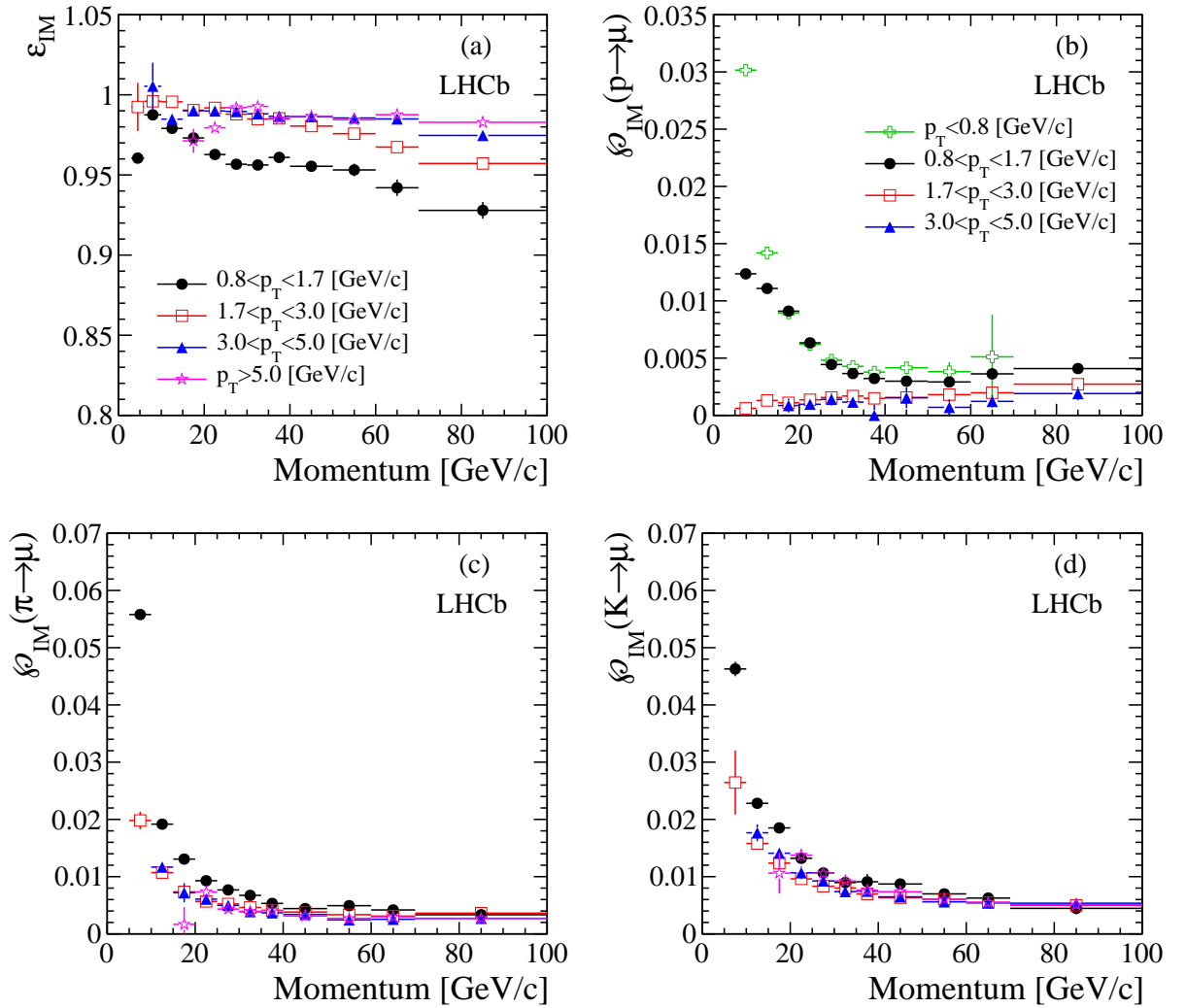


Figure 5: IsMuon efficiency and misidentification probabilities, as a function of momentum, in ranges of transverse momentum: ϵ_{IM} (a), $\phi_{IM}(p \rightarrow \mu)$ (b), $\phi_{IM}(\pi \rightarrow \mu)$ (c) and $\phi_{IM}(K \rightarrow \mu)$ (d).

Table 2: Average IsMuon efficiency and misidentification probabilities in different transverse momentum intervals (%).

| p_T interval (GeV/c) | muon | proton | pion | kaon |
|-------------------------|------------------|-------------------|-----------------|-----------------|
| $p_T < 0.8$ | | 1.393 ± 0.005 | 6.2 ± 0.1 | 4.3 ± 0.1 |
| $0.8 < p_T < 1.7$ | 96.94 ± 0.07 | 0.737 ± 0.003 | 2.19 ± 0.01 | 1.93 ± 0.1 |
| $1.7 < p_T < 3.0$ | 98.53 ± 0.05 | 0.149 ± 0.004 | 0.61 ± 0.01 | 0.93 ± 0.01 |
| $3.0 < p_T < 5.0$ | 98.51 ± 0.06 | 0.12 ± 0.02 | 0.40 ± 0.01 | 0.72 ± 0.01 |
| $5.0 < p_T$ | 98.51 ± 0.07 | | 0.33 ± 0.02 | 0.69 ± 0.01 |

225 0.2-5.6% and 0.6-4.5%, respectively. For momentum above 30 GeV/c, $\wp_{IM}(\pi \rightarrow \mu)$ and
 226 $\wp_{IM}(K \rightarrow \mu)$ have a small dependence on p_T . At the lowest p_T range, the kaon
 227 misidentification probability is lower than the pion for the lowest momentum interval,
 228 in spite of the larger decay width of kaons to muons. Since the muon is produced with a
 229 larger opening angle with respect to the original track trajectory in kaon decays than in
 230 pion decays, and on average low momentum particles tend to decay further upstream in
 231 the detector, then the hits in the muon chambers have a higher probability to lie outside
 232 the fields of interest.

233 When integrated over $p > 3$ GeV/c and the whole p_T spectra of our calibration sam-
 234 ples, the average values for the misidentification probabilities are $\wp_{IM}(p \rightarrow \mu) = (1.033$
 235 $\pm 0.003)\%$, $\wp_{IM}(\pi \rightarrow \mu) = (1.025 \pm 0.003)\%$ and $\wp_{IM}(K \rightarrow \mu) = (1.111 \pm 0.003)\%$. For pi-
 236 ons and kaons, about 60% of the misidentification probability is due to decays in flight,
 237 for these particular samples. The average efficiency and misidentification probabilities,
 238 integrated over momentum ($p > 3$ GeV/c), are also given in Table 2, for 5 different p_T
 239 intervals. There are not enough candidates in the muon, pion and kaon samples for a
 240 measurement dependent on momentum in the lowest p_T bin. Similarly for the protons,
 241 in the highest p_T interval.

242 The LHCb detector has been designed to operate at the luminosity of $\mathcal{L} = 2 \times$
 243 $10^{32} \text{ cm}^{-2} \text{ s}^{-1}$ and with a probability of having one interaction per beam crossing max-
 244 imal with respect to higher numbers. However, in the 2011 run the experiment operated
 245 with an average number of interactions per beam crossing about 2.5 times the nominal
 246 average, with a corresponding increase of the overall detector occupancies. The behavior
 247 of ε_{IM} and \wp_{IM} was then evaluated as a function of the number of tracks which contain
 248 hits in the tracking subsystems, from the VELO to the tracking stations. No signifi-
 249 cant decrease of ε_{IM} is observed, while an increase of the misidentification probabilities
 250 is seen with higher track multiplicities, as expected. The detailed behaviour of both the
 251 efficiency and the misidentification probabilities as a function of momentum is shown in
 252 Fig. 6. The probability $\wp_{IM}(p \rightarrow \mu)$ increases by a factor 2.7 for particles with momentum
 253 in the range 3 to 5 GeV/c, when comparing events with track multiplicity smaller than 40
 254 and events with track multiplicity between 150 and 250, which is the highest interval of
 255 multiplicity analysed. At high momentum, the difference is much less pronounced. For
 256 pions and kaons, the increase at low momentum is a factor of two, approximately, and

257 drops quickly to a plateau value starting at 20 GeV/c. Since the FOI are smaller at high
 258 momentum, the misidentification probability becomes less sensitive to the multiplicity of
 259 the underlying event.

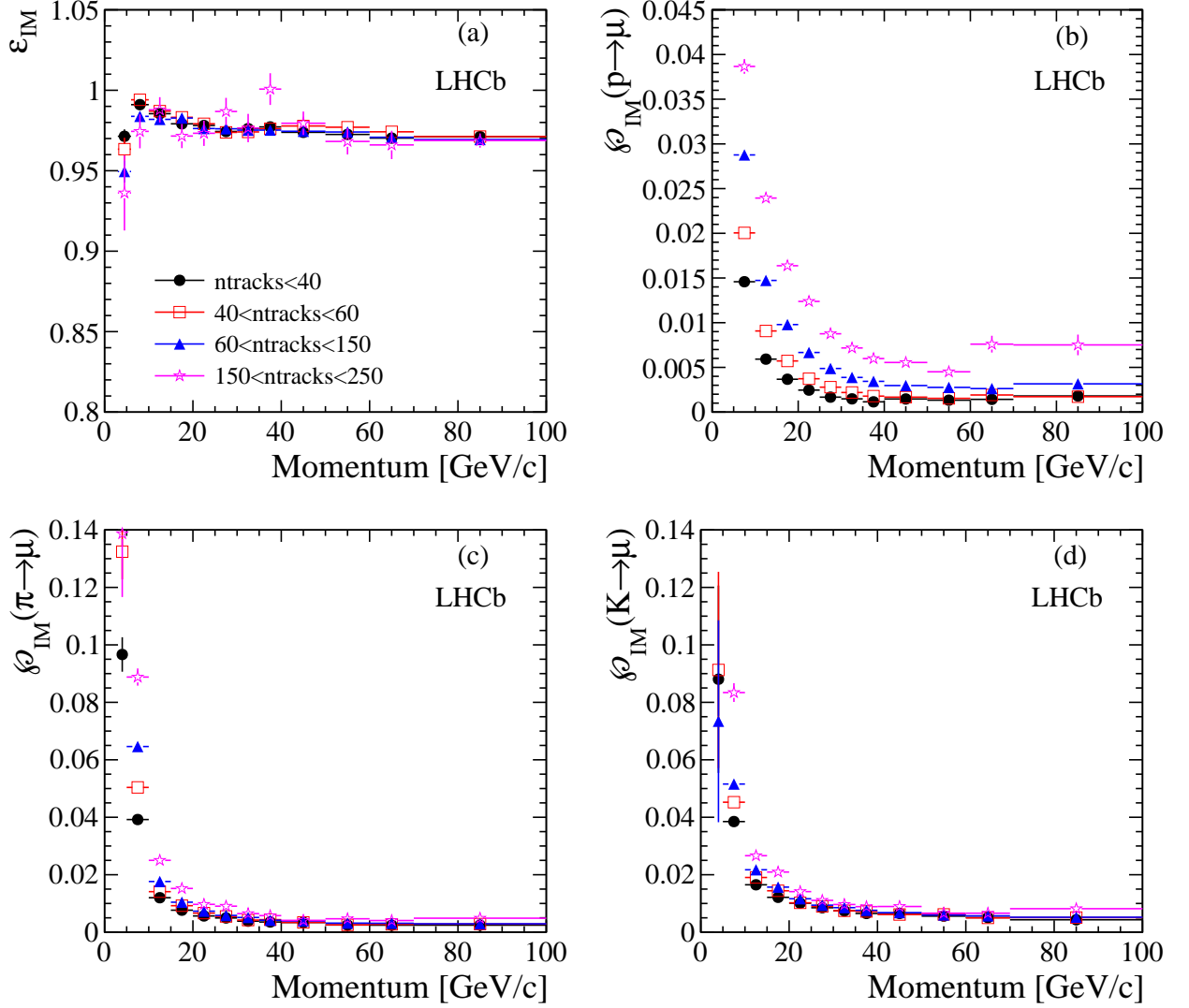


Figure 6: IsMuon efficiency ε_{IM} (a) and \wp_{IM} for protons (b), pions (c) and kaons (d) as a function of momentum for different ranges of the number of trajectories reconstructed in the event (n_{tracks}).

260 The charge dependence of the efficiency ε_{IM} is also analysed. No difference between
 261 the efficiencies is seen up to the level of the statistical fluctuations. When integrating over
 262 the whole momentum range, the relative difference is $0.09 \pm 0.08\%$, compatible with zero
 263 within the statistical uncertainty.

264 5.2 Muon likelihoods

265 The muon identification efficiency ($\varepsilon_{\text{muDLL}}$) is measured as a function of a selection cut
266 in the variable muDLL, for different momentum ranges, as shown in Fig. 7(a). The
267 misidentification probabilities are also shown in Fig. 7(b) to Fig. 7(d), for the same mo-
268 mentum ranges. The black solid line shows the average fractions, when integrated over
269 $p > 3 \text{ GeV}/c$ (and $p_T > 0.8 \text{ GeV}/c$ for the muons). All curves start at the efficiency or
270 misidentification probability corresponding to the IsMuon requirement. For tracks with
271 $p > 10 \text{ GeV}/c$, the muon efficiency is independent of momentum up to $\text{muDLL} \sim 2$. To
272 achieve a misidentification probability independent from the momentum, the value of
273 the muDLL cut must depend on particle momentum. By applying a muDLL cut irre-
274 spective of the momentum, the misidentification probabilities show a strong momentum
275 dependence.

276 As an example, when requiring $\text{muDLL} \geq 1.74$, a cut that provides a final muon ef-
277 ficiency of 93.2%, the final misidentification probabilities are 0.21%, 0.78% and 0.52%
278 for protons, kaons and pions respectively. This cut, which provides a sharp decrease of
279 5% of the efficiency with respect to the IsMuon efficiency, is used here as an example
280 only for a clear comparison between the muon DLL and the DLL. Since the average ef-
281 ficiency and misidentification probabilities values are given for our calibration samples,
282 which have their particular momentum and p_T spectrum, they can be different for samples
283 with different kinematic distributions.

284 The momentum dependence of $\varepsilon_{\text{muDLL}}$ and of \wp_{muDLL} for particles satisfying this cut
285 are shown in Fig. 8, compared to the IsMuon requirement alone and a tighter cut,
286 $\text{muDLL} \geq 2.25$. Again, this second cut was chosen for providing a sharp reduction of
287 the muon efficiency of 10% with respect to the IsMuon efficiency. Once more, since the
288 performance is integrated over p_T , small variations from these values are expected for
289 different samples, in particular for the misidentification probabilities, which present a
290 stronger dependence with transverse momentum.

291 5.3 Combined likelihoods

292 The DLL efficiency is shown as a function of the pion and kaon
293 misidentification probabilities in Fig. 9, together with the results obtained using
294 the muDLL alone, allowing for a direct comparison of their performances.

295 The DLL benefits from RICH and calorimeter information, being more effective than
296 the muon DLL alone in separating pions and kaons from muons. After IsMuon, this
297 is the most used particle identification requirement used to select muons in LHCb and
298 the actual cut value is usually chosen according to the compromise between purity and
299 efficiency needed for that specific study. The average misidentification rates corresponding
300 to a cut which provides an average decrease of 5% (equivalent to the one obtained with
301 $\text{muDLL} \geq 1.74$, as previously shown) are around 0.65% and 0.38% for the kaons and pions,
302 respectively.

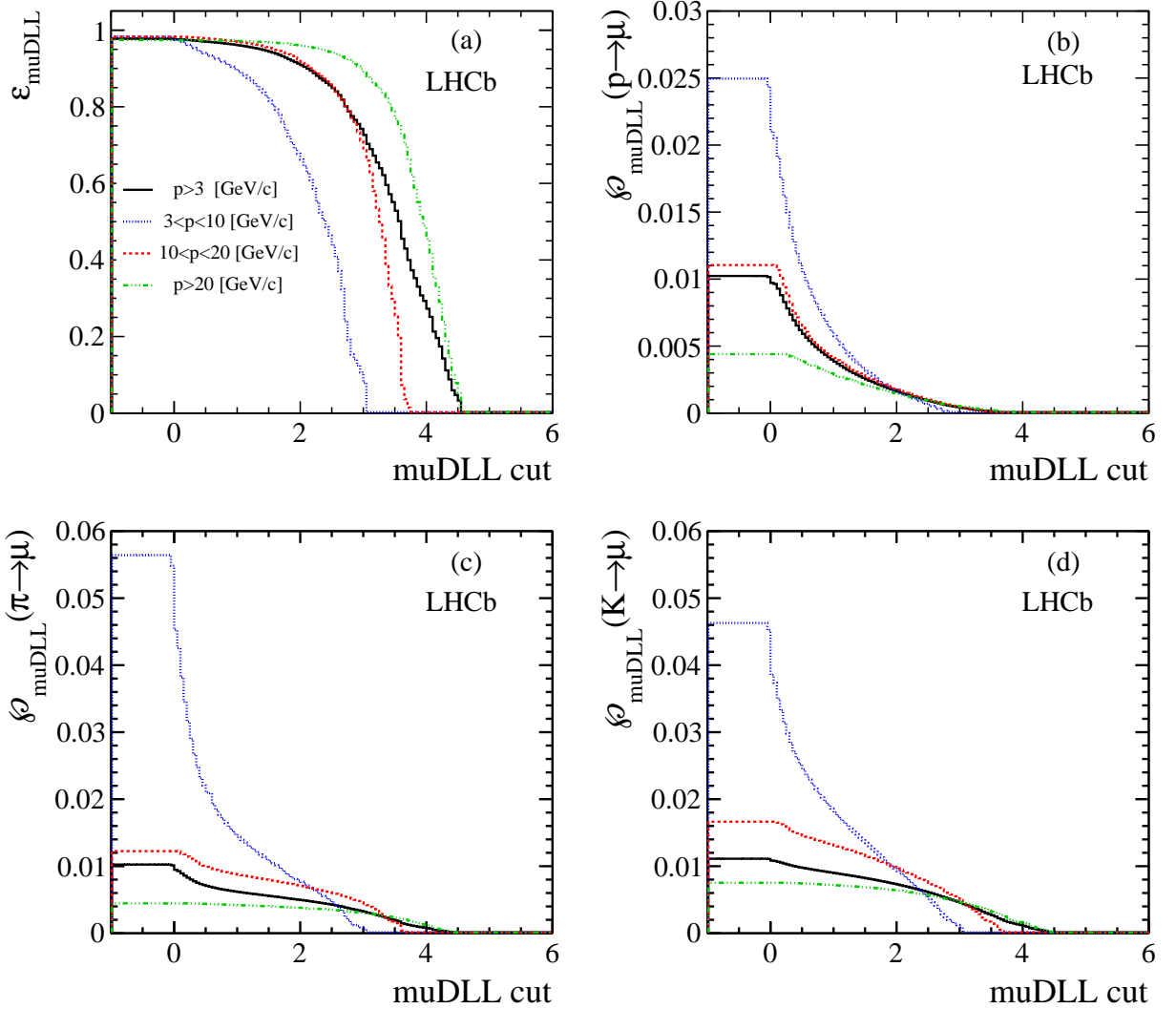


Figure 7: The efficiency $\varepsilon_{\text{muDLL}}$ as a function of muon DLL cut for muons (a) and misidentification probabilities for protons (b), pions (c) and kaons (d). The black solid line shows the average values integrated over $p > 3 \text{ GeV}/c$. The blue dotted line correspond to particles in the range $3 < p < 10 \text{ GeV}/c$. The red dashed lines show results for $10 < p < 20 \text{ GeV}/c$ and the green dashed-dotted for $p > 20 \text{ GeV}/c$.

303 5.4 Performance of selections based on hits sharing

304 As mentioned in Section 3, after requiring IsMuon, an additional way of reducing the
 305 incorrect identification probability of hadrons as muons, in particular at high occupancy,
 306 is the use of a cut on NShared.

307 The muon efficiency is shown as a function of the pion misidentification probability
 308 for corresponding NShared cut in Fig. 10(a); protons are shown in Fig. 10(b). Due to
 309 similar decay-in-flight pollution at low momentum, kaons behave as pions. The black

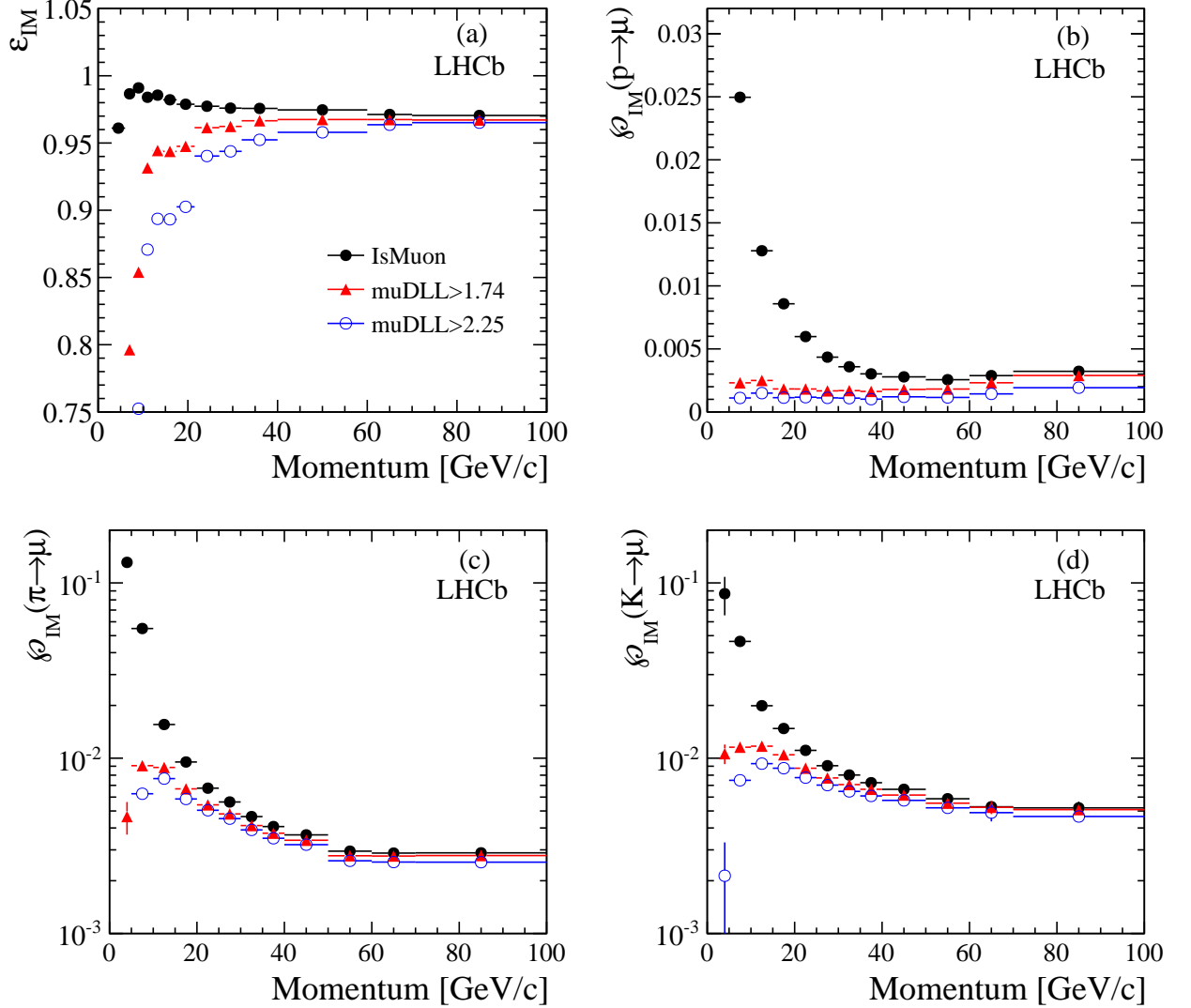


Figure 8: Muon efficiency (a) and misidentification probabilities for protons (b), pions (c) and kaons (d) as a function of the particle momentum for the IsMuon requirement alone (black solid circles) and with the additional cuts $\text{muDLL} \geq 1.74$ (red triangles) and $\text{muDLL} \geq 2.25$ (blue open circles).

310 solid line shows the average values integrated over $p > 3$ GeV/c. The NShared selection
 311 is particularly effective at low momenta, with increasing the FOI size.

312 5.5 Systematic checks

313 The effect of the trigger and of the method chosen to evaluate the efficiency and
 314 misidentification probabilities are investigated.

315 Alternatively to the requirement of the $J/\psi \rightarrow \mu^+ \mu^-$ sample being triggered indepen-

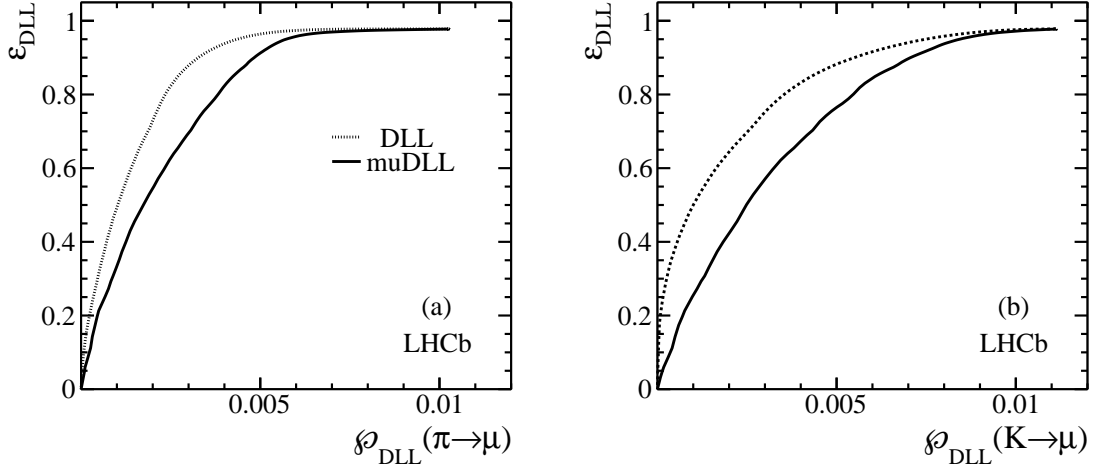


Figure 9: Average efficiency ε_{DLL} as a function of the pion (a) and kaon (b) misidentification probabilities for particles with momentum in the range $p > 3 \text{ GeV}/c$. The dotted lines show the DLL performance, while the muon DLL performance is shown with a solid line.

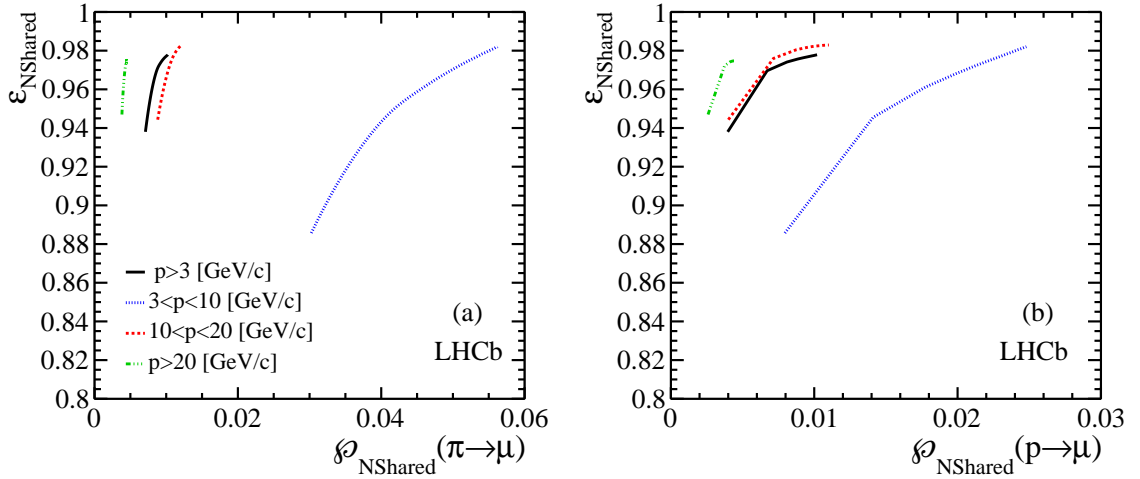


Figure 10: Muon efficiency $\varepsilon_{\text{NShared}}$ as a function of the pion and proton misidentification probabilities. The average values, for all particles with $p > 3 \text{ GeV}/c$, are shown with a black line, compared to the three momentum ranges separately, as for Fig. 7.

316 dently of the probe muon, a muon trigger decision based on the tag muon was used to
 317 evaluate the IsMuon efficiency. The systematic uncertainty due to the choice of trigger
 318 strategy is taken as the difference between the two determinations, which is 0.2%.

319 When performing a full fit to the signal and background components of the mass
 320 distributions used to extract the yields of signal events satisfying or not the muon iden-

321 tification requirements, the resulting efficiencies and proton misidentification probability
322 rates agree within the statistical uncertainties with the results shown in Section 5.

323 For the pion and kaon misidentification probabilities, the effect of the trigger is studied
324 and found to be negligible within the uncertainties, independently of momentum and
325 transverse momentum. Also the systematic uncertainty related to the method used for
326 the evaluation of the efficiency is found to be negligible as a function of momentum, apart
327 from a few intervals where it is comparable with the statistical accuracy.

328 **6 Conclusions**

329 The performance of the muon identification procedure used in the LHCb experiment has
330 been evaluated, using a dataset corresponding to 1 fb^{-1} recorded in 2011 at $\sqrt{s} = 7 \text{ TeV}$.

331 A loose binary criterium that can be used to select muons is based on the matching
332 of muon hits with the particle trajectory. For candidates satisfying this requirement,
333 likelihoods for muon and non-muon hypotheses are built with the pattern of hits around
334 the trajectories, which can be used to refine the selection. An additional way of rejecting
335 fake muon candidates is provided by a variable sensitive to hit sharing by nearby particles.

336 The muon identification efficiency was observed to be robust against the variation
337 of detector occupancies and presents a weak dependence on momentum and transverse
338 momentum. Hadron misidentification probabilities present a stronger dependence on hit
339 or track multiplicity, however the highest increase factors are observed only for low mo-
340 mentum particles.

341 Average muon identification efficiencies at the 98% level are attainable for pion and
342 kaon misidentification below the 1% level at high transverse momentum, using the loosest
343 identification criterium. The performance of additional requirements based on likelihoods
344 or on hits sharing can be tuned according to the needs of each analysis and reduce the
345 misidentification probabilities dependence on track multiplicity. Adding a requirement on
346 the difference of the log-likelihoods that provides a total muon efficiency at the level of
347 93%, the hadron misidentification probabilities are below 0.6%.

348 **Acknowledgements**

349 We express our gratitude to our colleagues in the CERN accelerator departments for
350 the excellent performance of the LHC. We thank the technical and administrative staff at
351 CERN and at the LHCb institutes, and acknowledge support from the National Agencies:
352 CAPES, CNPq, FAPERJ and FINEP (Brazil); CERN; NSFC (China); CNRS/IN2P3
353 (France); BMBF, DFG, HGF and MPG (Germany); SFI (Ireland); INFN (Italy); FOM
354 and NWO (The Netherlands); SCSR (Poland); ANCS (Romania); MinES of Russia and
355 Rosatom (Russia); MICINN, XuntaGal and GENCAT (Spain); SNSF and SER (Switzer-
356 land); NAS Ukraine (Ukraine); STFC (United Kingdom); NSF (USA). We also acknowl-
357 edge the support received from the ERC under FP7 and the Region Auvergne.

References

- 358
- 359 [1] LHCb collaboration, A. A. Alves Jr. *et al.*, *The LHCb detector at the LHC*, JINST
360 **3** (2008) S08005.
- 361 [2] LHCb collaboration, R. Aaij *et al.*, *First evidence for the decay $B_s^0 \rightarrow \mu^+\mu^-$* , Phys.
362 Rev. Lett. **110** (2013) 021801, [arXiv:1211.2674](#).
- 363 [3] LHCb collaboration, R. Aaij *et al.*, *Measurement of the isospin asymmetry in $B \rightarrow$*
364 *$K^{(*)}\mu^+\mu^-$ decays*, J. High Energy Phys. **07** (2012) 133, [1205.3422](#).
- 365 [4] LHCb collaboration, R. Aaij *et al.*, *Differential branching fraction and angular*
366 *analysis of the decay $B^0 \rightarrow K^{*0}\mu^+\mu^-$* , Phys. Rev. Lett. **108** (2011) 181806,
367 [arXiv:1112.3515](#).
- 368 [5] LHCb collaboration, R. Aaij *et al.*, *Measurement of the $B_s^0 \rightarrow J/\psi\bar{K}^{*0}$ branching*
369 *fraction and angular amplitudes*, Phys. Rev. D **86** (2012) 071102, [arXiv:1208.0738](#).
- 370 [6] LHCb collaboration, R. Aaij *et al.*, *Measurement of the cp -violating phase ϕ_s in the*
371 *decay $B_s^0 \rightarrow J/\psi\phi$* , Phys. Rev. Lett. **108** (2011) 101803, [1112.3183](#).
- 372 [7] LHCb collaboration, R. Aaij *et al.*, *Measurement of the cp violating phase ϕ_s in*
373 *$\bar{B}_s^0 \rightarrow J/\psi f_0(980)$* , Phys. Lett. B **707** (2011) 497505, [1112.3056](#).
- 374 [8] A. A. Alves Jr. *et al.*, *Performance of the LHCb muon system*, JINST **8** (2013)
375 P02022, [arXiv:1112.1346](#).
- 376 [9] R. Aaij and J. Albrecht, *Muon triggers in the High Level Trigger of LHCb*, LHCb-
377 PUB-2011-017 (2011).
- 378 [10] M. Clemencic *et al.*, *The LHCb simulation application, GAUSS: design, evolution*
379 *and experience*, J. Phys: Conf. Ser. **331** (2011) 032023.
- 380 [11] C. Grupen, *Particle Detectors*. Cambridge university press, Cambridge, England,
381 1996.
- 382 [12] M. Adinolfi *et al.*, *Performance of the LHCb RICH detector at the LHC*,
383 [arXiv:1211.6759](#).
- 384 [13] R. Aaij *et al.*, *The LHCb Trigger and its Performance*, JINST **8** (2012) P04022,
385 [arXiv:1211.3055](#).